

A detectable ultra-high-energy cosmic ray outburst from GRB 221009A

HAO-NING HE,^{1,2} B. THOEDORE ZHANG,³ AND YI-ZHONG FAN^{1,4}

¹*Key Laboratory of Dark Matter and Space Astronomy, Purple Mountain Observatory, Chinese Academy of Sciences, Nanjing 210023, China*

²*Astrophysical Big Bang Laboratory, RIKEN, Wako, Saitama 351-0198, Japan*

³*Center for Gravitational Physics and Quantum Information, Yukawa Institute for Theoretical Physics, Kyoto University, Kyoto 606-8502, Japan*

⁴*School of Astronomy and Space Science, University of Science and Technology of China, Hefei 230026, China*

ABSTRACT

Gamma-ray bursts (GRBs) have been proposed as one of promising sources of ultra-high-energy cosmic rays (UHECRs), but observational evidence is still lacking. The nearby B.O.A.T. (brightest of all time) GRB 221009A, an once-in-1000-year event, is able to accelerate protons to $\sim 10^3$ EeV. Protons arriving at the Milky Way are dominated by neutron-decay-induced protons. The inter-galactic magnetic fields would not yield a sizable delay of the ≥ 10 EeV cosmic rays if its strength is $\lesssim 10^{-13}$ G, while Galactic magnetic fields would cause a significant time delay. We predict that, an UHECR burst from GRB 221009A would be detectable by the Pierre Auger Observatory and the TA \times 4, within ~ 10 years. The detection of such an UHECR outburst will provide the direct evidence for UHECR acceleration in GRBs.

Keywords: Gamma-ray bursts (629) — Cosmic rays (329) — Extragalactic magnetic fields (507) — Cosmic ray sources (328) — High energy astrophysics (739)

1. INTRODUCTION

The origin of the highest energy cosmic particles is still in debate. GRBs, the most luminous phenomenon in the universe, are proposed as one of the most promising sources of UHECRs (Waxman 1995; Vietri 1995). However, no observed UHECRs or TeV-PeV neutrinos have been confirmed to be associated with GRBs (Icecube Collaboration et al. 2012; Abbasi et al. 2022). One of the difficulties of identifying UHECRs associated with GRBs is the deflections and the consequent time delays caused by the magnetic fields. The magnetic deflection angles and the delay times are dependent on the distance of GRBs and the properties of the interstellar (both in the host galaxy and the Galaxy) and inter-galactic magnetic fields. What's more, UHECRs would lose a good fraction of energy via interacting with the extragalactic background light (EBL) and cosmic microwave background (CMB) photons during the propagation, implying that distant GRBs can hardly contribute to UHECRs. In addition, the pointing direction of the GRB jet, the capability of accelerating UHECRs, the total energy deposited into CRs, and the escape rate of UHECRs from the burst and the host galaxy are also key issues for the nearby individual GRB (Mészáros 2002; Kumar & Zhang 2015).

GRB 221009A, locating at $z = 0.151$ (the luminosity distance of 745 Mpc (Malesani et al. 2023)) and releasing an isotropic-equivalent radiation energy of $E_{\gamma, \text{iso}} \simeq 10^{55}$ ergs (An et al. 2023), is the brightest of all time (B.O.A.T.) (Pillera et al. 2022; de Ugarte Postigo et al. 2022; Castro-Tirado et al. 2022; Malesani et al. 2023; Levan et al. 2023). Throughout this work, the convention $Q_x = Q/10^x$ is adopted. It is also the first GRB with photons of energy extending up to ~ 10 TeV (Cao et al. 2023a,b), indicating its potential ability of accelerating UHECRs (Mirabal 2023; Alves Batista 2022; Das & Razzaque 2023; Zhang et al. 2023a,b; Isravel et al. 2023). Likely, only 1 of 10,000 randomly generated long bursts is as energetic as GRB 221009A, and the rate of GRBs as nearby and as energetic as GRB

221009A is $\lesssim 1$ per 1000 years (Burns et al. 2023; Williams et al. 2023). Therefore, GRB 221009A provides us a precious opportunity to study UHECRs in our life time.

The energy dissipation radius of this GRB is large, i.e., $R = 2\Gamma^2 ct_v / (1+z) = 10^{15} \text{ cm } (1+z)^{-1} \Gamma_{2.7}^2 \frac{t_v}{0.082 \text{ s}}$, where the variability timescale is measured as $t_v = 0.082 \text{ s}$ (Liu et al. 2023), based on the *Fermi*-GBM data from 210 s to 219 s after the *Fermi*-GBM trigger, and c is the speed of light. The bulk Lorentz factor Γ suggested by LHAASO observations on the afterglow is also large (Cao et al. 2023a). The large energy dissipation radius and the large bulk Lorentz factor Γ favor a large maximum acceleration energy of protons. If protons are accelerated at the energy dissipation radius during the prompt emission phase, the photomeson production interaction and the Bethe-Heitler pair production process between accelerated protons and prompt photons will produce neutrons, neutrinos, and electromagnetic particles initiating electromagnetic cascades (contributing to GeV-TeV photons) (Böttcher & Dermer 1998; Dermer & Atoyan 2006; Wang et al. 2018). The non-detection of neutrinos by the IceCube observatory, observations on GeV photons by *Fermi*-LAT, and observations on VHE photons by LHAASO set constraints on the acceleration and interaction mechanism of protons (Abbasi et al. 2023; Veres et al. 2022; Bissaldi et al. 2022; Ai & Gao 2023; Murase et al. 2022; Liu et al. 2023; Rudolph et al. 2023; Wang et al. 2023). The tightest constraint is made by (Wang et al. 2023) based on LHAASO observations, and the baryon loading factor is constrained to be $\xi_p \equiv E_p / E_{\gamma, \text{iso}} \leq 2$ for a Lorentz factor $\Gamma = 500$, suggesting a possible high isotropic energy deposited in protons (E_p). LHAASO's observations on the afterglow emission suggest that the jet of GRB 221009A is pointing to Earth. The fact that the jet pointing to Earth allows the accelerated UHECRs to propagate to the direction of Earth.

In aggregate, the specific features of the B.O.A.T. GRB 221009A, such as the large energy dissipation radius, the large bulk Lorentz factor, the high isotropic energy, and the jet pointing to Earth, favor the burst as a possible UHECR source. To answer the question of whether the UHECR burst from GRB 221009A can be detected in our life time, we study the acceleration and escape of UHECRs in the burst, and simulate the propagation of UHECRs from the burst. Since the jet composition of high-luminosity GRBs is likely to be dominated by protons (Zhang et al. 2018), throughout this work, we assume the composition of UHECRs from the GRB is pure proton.

2. THE ACCELERATION AND ESCAPE OF PROTONS

Since most of the radiation energy is released via the prompt emission during the brightest emission phase from 225.024 s to 233.216 s after the Konus-WIND trigger time in the second pulse (Frederiks et al. 2023), we assume most of the UHECRs are accelerated during the brightest emission phase in the second pulse as well. Parameters of the prompt emission for the brightest phase in the second pulse are listed in Table 1. Protons are expected to be accelerated at the energy dissipation radius within the dynamic time, and meantime are undergoing energy loss due to the synchrotron emission, the hadronic interaction with prompt photons.

The dynamic timescale is $t'_{\text{dyn}} = R/(c\Gamma) \simeq 67 \text{ s } R_{15} \Gamma_{2.7}^{-1}$. The magnetic field at the energy dissipation radius can be calculated by assuming the energy fraction of the magnetic field and electrons as ϵ_B and ϵ_e , i.e., $B' = (8\pi\epsilon_B L_\gamma / (\epsilon_e 4\pi R^2 \Gamma^2 c))^{1/2} \simeq 5.2 \times 10^3 \text{ G } \epsilon_{e,-1}^{-\frac{1}{2}} \epsilon_{B,-2}^{\frac{1}{2}} \Gamma_{2.7}^{-1} R_{15}^{\frac{1}{2}} L_{\gamma,54}^{\frac{1}{2}}$, where L_γ is the calibration luminosity. The acceleration timescale of protons with energy of ϵ_p is $t'_{\text{acc}}(\epsilon_p) = R'_L(\epsilon_p)/c \simeq 4.9 \text{ s } (1+z) \epsilon_{p,20} \eta_0^{-1} \epsilon_{e,-1}^{\frac{1}{2}} \epsilon_{B,-2}^{-\frac{1}{2}} R_{15} L_{\gamma,54}^{-\frac{1}{2}}$. The synchrotron cooling time scale of protons is $t'_{\text{syn}}(\epsilon_p) = 9m_p^4 \Gamma / (4ce^4 B'^2 \epsilon_p (1+z)) \simeq 7.3 \times 10^2 \text{ s } (1+z)^{-1} \epsilon_{p,20}^{-1} \epsilon_{e,-1} \epsilon_{B,-2}^{-1} \Gamma_{2.7}^3 R_{15}^2 L_{\gamma,54}^{-1}$, where m_p is the rest mass of protons.

The number density of the GRB prompt photons is described by $\frac{dn(\epsilon_\gamma)}{d\epsilon_\gamma} = A_\gamma \left(\frac{\epsilon_\gamma}{\epsilon_{\gamma,b}} \right)^{-q}$ where the normalization factor is $A_\gamma \sim L_\gamma / (4\pi c R^2 2\epsilon_{\gamma,b}^2)$, with $q = \alpha$ for $\epsilon_\gamma < \epsilon_{\gamma,b}$, $q = \beta$ for $\epsilon_\gamma > \epsilon_{\gamma,b}$. Adopting the Δ resonance approximation, the cross section peaks when the energy of photons is $\epsilon_{\gamma,\Delta} \simeq 0.3 \text{ GeV}$ in the proton rest frame. The energy loss timescale of the photomeson production interaction between protons and prompt photons is approximated to be (Waxman & Bahcall 1997; He et al. 2012)

$$t_{p\gamma}^{-1}(\epsilon_p) \simeq 5.3 \times 10^{-3} \text{ s}^{-1} (1+z)^{-1} L_{\gamma,54} R_{15}^{-2} \Gamma_{2.7}^{-1} \epsilon_{\gamma,b,3\text{MeV}}^{-1} \quad (1)$$

$$\times \begin{cases} \left(\frac{\epsilon_p}{\epsilon_{p,b}} \right)^{\beta-1}, & \epsilon_p < \epsilon_{p,b} \\ \left(\frac{\epsilon_p}{\epsilon_{p,b}} \right)^{\alpha-1}, & \epsilon_p > \epsilon_{p,b} \end{cases}$$

where $\epsilon_{p,b} \equiv \Gamma^2 \epsilon_{\gamma,\Delta} m_p c^2 / (2(1+z)^2 \epsilon_{\gamma,b}) \simeq 8.9 \times 10^{15} \text{ eV } \Gamma_{2.7}^2 (1+z)^{-2} \epsilon_{\gamma,b,3\text{MeV}}^{-1}$ is the characteristic energy of protons that interacting with photons of energy $\epsilon_{\gamma,b}$ via Δ resonance.

Adopting parameters summarized in Table 1, the acceleration timescale, the energy loss timescales, and the dynamic time of protons at the energy dissipation radius are calculated and plotted in Figure 1. The curve of the energy loss timescale via the photomeson interaction is calculated numerically, since the analytical approximation shown in Eq. (1) is not accurate for protons at the high energy end, where the multi-pion channel plays an important role.

By comparing the dynamic timescale t'_{dyn} , the proton synchrotron cooling timescale t'_{syn} , the photomeson production timescale $t'_{p\gamma}$ with the proton acceleration timescale t'_{acc} , i.e., setting $\min[t'_{\text{dyn}}, t'_{\text{syn}}(\varepsilon_{p,\text{max}}), t'_{p\gamma}(\varepsilon_{p,\text{max}})] = t'_{\text{acc}}(\varepsilon_{p,\text{max}})$, we can estimate the maximum energy of the accelerated protons $\varepsilon_{p,\text{max}}$. As shown in Figure 1, we have $t_{\text{syn}}(\varepsilon_{p,\text{max}}) = t'_{\text{acc}}(\varepsilon_{p,\text{max}}) < t'_{\text{dyn}} < t'_{p\gamma}(\varepsilon_{p,\text{max}})$, and the maximum energy of accelerated protons is

$$\varepsilon_{p,\text{max}} = 1.2 \times 10^{21} \text{eV} (1+z)^{-1} \Gamma_{2.7}^{3/2} \eta_0^{1/2} \epsilon_{e,-1}^{1/4} \epsilon_{B,-2}^{-1/4} R_{15}^{1/2} L_{\gamma,54}^{-1/4}, \quad (2)$$

with η as the acceleration efficiency.

Protons with lower energy will be confined in the acceleration site due to the strong magnetic field. Those protons with the Larmor radius $R'_L(\varepsilon_p)$ and the cooling scale of the photomeson interaction $ct'_{p\gamma}(\varepsilon_p)$ larger than the shell thickness $\Delta r'$, would be able to escape directly. The escape rate of protons with energy of ε_p is estimated as (Baerwald et al. 2013)

$$f_{\text{esc}} = \lambda'_{\text{mfp}}(\varepsilon_p) / \Delta r' = \min[\Delta r', R'_L(\varepsilon_p), ct'_{p\gamma}(\varepsilon_p)] / \Delta r' \quad (3)$$

where $\lambda'_{\text{mfp}}(\varepsilon_p) \equiv \min[\Delta r', R'_L(\varepsilon_p), ct'_{p\gamma}(\varepsilon_p)]$ is the mean free path of protons with energy of ε_p . The shell thickness is $\Delta r' \simeq \Gamma ct_v / (1+z) = 1.2 \times 10^{12} \text{cm} (1+z)^{-1} \Gamma_{2.7} \frac{t_v}{0.082 \text{s}}$, the Larmor radius of protons is $R'_L(\varepsilon_p) = \varepsilon_p (1+z) / (\Gamma \eta e B') = 1.3 \times 10^{12} \text{cm} (1+z) \varepsilon_{p,21} \eta_0^{-1} \epsilon_{e,-1}^{\frac{1}{2}} \epsilon_{B,-2}^{-\frac{1}{2}} R_{15} L_{\gamma,54}^{-\frac{1}{2}}$, and e as the elementary charge. For protons with energy $\varepsilon_p > \varepsilon_{p,\text{esc}} = 9.6 \times 10^{20} \text{eV} (1+z)^{-2} \Gamma_{2.7} \eta_0 \epsilon_{e,-1}^{-\frac{1}{2}} \epsilon_{B,-2}^{\frac{1}{2}} R_{15}^{-1} L_{\gamma,54}^{\frac{1}{2}} \frac{t_v}{0.082 \text{s}}$, there are $\Delta r' < R'_L$ and $\Delta r' < ct'_{p\gamma}$. According to Eq. (3), the escape efficiency is $f_{\text{esc}} = 1$ for protons with energy $\varepsilon_p > \varepsilon_{p,\text{esc}}$ ¹.

Such escaped protons will be deflected by magnetic fields in the host galaxy. The deflection caused by the regular magnetic field in the host galaxy is dependent on the GRB location in the host galaxy and the pointing direction of the GRB jet. The Hubble space telescope observations reveal a disk-like host galaxy with an effective radius of about $R_e = 2.45 \pm 0.20 \text{kpc}$ (Levan et al. 2023). The host galaxy is viewed close to edge on with the burst about 0.65 kpc offset from the nucleus (Levan et al. 2023). Therefore, deflections on protons by the regular magnetic field in the host galaxy is approximated to be (Finley 2006)

$$\theta_{\text{reg,hg}} \simeq 4.1^\circ \varepsilon_{p,19.5}^{-1} \frac{B_{\text{reg,hg}}}{1 \mu\text{G}} \frac{R_e}{2.45 \text{kpc}}, \quad (4)$$

with $B_{\text{reg,hg}}$ is the average strength of the regular magnetic field. The root mean square (rms) of random deflections due to the turbulent magnetic field in the host galaxy is approximated as (Lee et al. 1995; Harari et al. 2002; Finley 2006)

$$\theta_{\text{rms,hg}} \simeq 1.5^\circ \varepsilon_{p,19.5}^{-1} \frac{B_{\text{rms,hg}}}{2 \mu\text{G}} \left(\frac{\lambda_{B,\text{hg}}}{50 \text{pc}} \right)^{1/2} \left(\frac{L_{\text{hg}}}{10 \text{kpc}} \right)^{1/2}, \quad (5)$$

where $B_{\text{rms,hg}}$ and $\lambda_{B,\text{hg}}$ are the rms strength and the coherent length of the turbulent magnetic field strength, and L_{hg} is the propagation length of protons in the turbulent magnetic field. The rms of the time delay due to the turbulent magnetic field is approximated as (Alcock & Hatchett 1978; Alves Batista 2022)

$$\Delta t_{\text{rms,hg}} \simeq \frac{L_{\text{hg}} \theta_{\text{rms,hg}}^2}{12c} \simeq 1.9 \text{yr} \varepsilon_{p,19.5}^{-2} \left(\frac{B_{\text{rms,hg}}}{2 \mu\text{G}} \right)^2 \frac{\lambda_{B,\text{hg}}}{50 \text{pc}} \left(\frac{L_{\text{hg}}}{10 \text{kpc}} \right)^2. \quad (6)$$

If only considering the deflection by the regular magnetic field and meanwhile $\theta_{\text{reg,hg}}$ is larger than the jet half-open angle θ_j , protons escaping from the host galaxy will not point to the Milky Way (MW). Taking account of the deflection by the turbulent magnetic field in the host galaxy and in the extragalactic field, a small fraction of protons might still have a chance to arrive at the MW. If $\theta_{\text{reg,hg}} < \theta_j$ and $\theta_{\text{rms,hg}} \gg \theta_j$, the flux of protons pointing to Earth would be reduced significantly. LHAASO's observation on the afterglow emission suggests a very narrow jet with a half-open

¹ To be noted here, we only consider the energy loss of protons due to interactions with prompt photons but ignore possible interactions with afterglow photons.

angle $\theta_j \simeq 0.6^\circ E_{k,55}^{-1/8} n_0^{1/8}$ (Cao et al. 2023a), where E_k is the isotropic kinetic energy and n is the circumstance density. If assuming $E_k = 3 \times 10^{55}$ erg, $n = 1$, $B_{\text{reg,hg}} = 1 \mu\text{G}$, $B_{\text{rms,hg}} = 2 \mu\text{G}$, $L_{\text{hg}} = 10$ kpc and $\lambda_{B,\text{hg}} = 50$ pc, for protons with energy $\varepsilon_p \gtrsim 300$ EeV, there are $\theta_{\text{reg,hg}} < \theta_j$ and $\theta_{\text{rms,hg}} < \theta_j$, indicating that protons with energy $\gtrsim 300$ EeV injected into the inter-galactic space from the host galaxy are still pointing to Earth. The rms of the time delay for $\gtrsim 300$ EeV protons is about 7 days, which will not affect the flux of detected protons in an observation time of a few years. If magnetic fields of the host galaxy are weaker, the threshold energy of protons pointing to Earth might be lower than 300 EeV. For the sake of conservation, we take account of protons with energy $\gtrsim 300$ EeV that directly escaping from the burst, as a component of UHECRs that injected into the inter-galactic space and propagating to the direction of Earth.

3. THE PRODUCTION AND ESCAPE OF NEUTRONS

Free neutrons are produced via the photomeson production interaction in the burst,

$$p + \gamma \rightarrow \Delta^+ \rightarrow \begin{cases} n + \pi^+ \\ p + \pi^0. \end{cases} \quad (7)$$

and would decay into protons via the β -decay, i.e.,

$$n \rightarrow p + e^- + \bar{\nu}_e, \quad (8)$$

with a lifetime of about $t'_n \simeq 879.6$ s in the rest frame (Workman et al. 2022).

The timescale for the neutron production is

$$t'_{p\gamma \rightarrow n} \simeq \frac{\kappa_{p\gamma}}{\rho \kappa_n \mathfrak{R}_n} t'_{p\gamma} \simeq 4.3 t'_{p\gamma}. \quad (9)$$

where $\rho = 0.23$ is the cross-section ratio, $\kappa_n = 0.4$ is the fraction of the proton energy converted into secondary neutrons, and $\mathfrak{R}_n = 1/2$ is the neutron multiplicity, for the target photon energy in the proton rest frame being larger than 2000 MeV (Mücke et al. 2000b; Mannheim et al. 2000; Dermer et al. 2012). Therefore, a fraction of the proton energy is converted into the neutron energy. The produced neutrons will lose energy via the $n\gamma$ interaction, with a cross section similar to that of $p\gamma$ interaction, i.e., $t'_{n\gamma} \simeq t'_{p\gamma}$. The optical thickness for neutron escape is $\tau_n \simeq (t'_{n\gamma} + t'^{-1}_{n\gamma})/t'^{-1}_{\text{dyn}} \simeq t'_{\text{dyn}}/t'_{p\gamma}$ (Baerwald et al. 2013). In the case of GRB 221009A, neutrons can escape from the burst since $\tau_n < 1$.

Ultra-high-energy neutrons with energy of ε_n will be able to travel a distance of

$$D_n = ct'_n \frac{\varepsilon_n(1+z)}{m_n} \simeq 88 \text{ kpc } \varepsilon_{n,19}(1+z) \quad (10)$$

before decaying into protons, which is considerably larger than the scale of most galaxies for $\varepsilon_n \gtrsim 10^{19}$ eV, where m_n is the rest mass of neutrons. Therefore, neutrons with energy larger than 10 EeV, produced in the photomeson production interactions, are able to escape from the host galaxy with no deflections or time delay, and then decay into protons in the inter-galactic space. The neutron-decay-induced protons will be an important component of UHECRs that injected into the inter-galactic space.

4. SPECTRA OF ACCELERATED PROTONS, ESCAPED PROTONS AND SECONDARY PARTICLES

Protons are assumed to be accelerated following a power-law spectrum with an exponential cutoff at the highest energy range,

$$\varepsilon_p^2 \frac{dN_p^{\text{acc}}}{d\varepsilon_p} = A_p \varepsilon_p^{-p+2} \exp(-\varepsilon_p/\varepsilon_{p,\text{max}}), \quad (11)$$

where the normalization coefficient $A_p = \xi_p E_{\gamma,\text{iso}} / \ln(\varepsilon_{p,\text{max}}/\varepsilon_{p,\text{min}})$ for $p = 2$, $\varepsilon_{p,\text{min}}$ is assumed to be the rest energy of protons. The luminosity of the total protons are $L_p = \xi_p L_\gamma = 10^{54} \text{ erg } \xi_{p,0} L_{\gamma,54}$. The adopted values of ξ_p , $E_{\gamma,\text{iso}}$, L_γ , $\varepsilon_{p,\text{max}}$ and $\varepsilon_{p,\text{min}}$ are listed in Table 1.

The spectrum of direct escaping protons can be approximated as

$$\varepsilon_p^2 \frac{dN_p^{\text{esc}}}{d\varepsilon_p} = \varepsilon_p^2 \frac{dN_p^{\text{acc}}}{d\varepsilon_p} f_{\text{esc}} = A_p \exp(-\varepsilon_p/\varepsilon_{p,\text{max}}) f_{\text{esc}}. \quad (12)$$

The production of secondaries from the photomeson production process are calculated via the following formula numerically,

$$\frac{dN_s}{d\varepsilon_s} = \int \frac{d\varepsilon_p}{\varepsilon_p} \frac{dN_p^{\text{acc}}}{d\varepsilon_p} \int d\varepsilon_\gamma \frac{dn_\gamma}{d\varepsilon_\gamma} \mathcal{R}(\varepsilon_s, \varepsilon_p), \quad (13)$$

where s denotes neutrons and neutrinos, and $\mathcal{R}(\varepsilon_s, \varepsilon_p)$ represents the production rate of secondary particles, including neutrons and neutrinos with energy ε_s , produced from primary protons with energy ε_p . The production rate table $\mathcal{R}(\varepsilon_s, \varepsilon_p)$ can be generated with the Monte Carlo generator SOPHIA (Mücke et al. 2000a). Parameters adopted in the calculation are listed in Table 1, following measurements and constraints based on the multi-messenger observations.

In the calculation, the synchrotron cooling of the secondary pions and muons (He et al. 2012) have been taken into account. Charged pions produced in the photomeson interaction will decay into 4 final state leptons, via processes $\pi^\pm \rightarrow \nu_\mu(\bar{\nu}_\mu)\mu^\pm \rightarrow \nu_\mu(\bar{\nu}_\mu)e^+(e^-)\nu_e(\bar{\nu}_e)\bar{\nu}_\mu(\nu_\mu)$, which approximately share the pion energy equally. The all flavor neutrino spectrum can be calculated as (He et al. 2012)

$$\epsilon_\nu \frac{dn_\nu}{d\epsilon_\nu} d\epsilon_\nu = \frac{3\Re(\epsilon_p)}{4} f_{p\gamma}(\epsilon_p) \theta_\nu(\epsilon_p) \epsilon_p \frac{dn_p}{d\epsilon_p} d\epsilon_p, \quad (14)$$

with the factor $\theta_\nu(\epsilon_p) = \frac{1}{3}\zeta_\pi(\epsilon_p) + \frac{2}{3}\zeta_\pi(\epsilon_p)\zeta_\mu(\epsilon_p)$ accounting for the cooling of secondary particles, where $\zeta_\pi = 1 - \exp(-t_{\pi, \text{syn}}/\tau_\pi)$ and $\zeta_\mu = 1 - \exp(-t_{\mu, \text{syn}}/\tau_\mu)$ are suppression factors caused by the synchrotron cooling of pions and muons, and \Re is the ratio between the amount of the charged pions and the total pions. The synchrotron cooling timescales of pions and muons can be calculated as $t_{\pi, \text{syn}} = 0.041 \text{ s } (1+z)^{-1} \epsilon_{\pi, 18}^{-1} \epsilon_{e, -1}^{-1} \epsilon_{B, -2}^{-1} \Gamma_{2.7}^3 R_{15}^2 L_{\gamma, 54}^{-1}$ and $t_{\mu, \text{syn}} = 0.015 \text{ s } (1+z)^{-1} \epsilon_{\mu, 18}^{-1} \epsilon_{e, -1}^{-1} \epsilon_{B, -2}^{-1} \Gamma_{2.7}^3 R_{15}^2 L_{\gamma, 54}^{-1}$, and the life time of pions and muons can be written as $\tau_\pi = 0.37 \text{ s } \epsilon_{\pi, 18} \Gamma_{2.7}^{-1} (1+z)$ and $\tau_\mu = 41.5 \text{ s } \epsilon_{\mu, 18} \Gamma_{2.7}^{-1} (1+z)$. The energy of pions and muons in the observer's frame are approximated to be $\epsilon_\pi \simeq 0.2\epsilon_p$ and $\epsilon_\mu = 0.15\epsilon_p$.

The characteristic cutoff energy of pions and muons due to the synchrotron cooling, can be calculated via equating the life time and the synchrotron cooling timescale, i.e.,

$$\epsilon_{\pi, \text{cut}} = 1.9 \times 10^{17} \text{ eV } (1+z)^{-1} \epsilon_{e, -1}^{1/2} \epsilon_{B, -2}^{-1/2} \Gamma_{2.7}^2 R_{15} L_{\gamma, 54}^{-1/2} \quad (15)$$

and

$$\epsilon_{\mu, \text{cut}} = 1.0 \times 10^{16} \text{ eV } (1+z)^{-1} \epsilon_{e, -1}^{1/2} \epsilon_{B, -2}^{-1/2} \Gamma_{2.7}^2 R_{15} L_{\gamma, 54}^{-1/2}. \quad (16)$$

In Figure 2, we plot the all-flavor neutrino fluence. The IceCube found none track-like events to the direction of the GRB from the fast-response analysis (FRA; IceCube Collaboration (2022); Abbasi et al. (2023)) in a time window of -1 hour to $+2$ hours from the *Fermi*-GBM trigger time, assuming a power law neutrino spectrum with different index p (IceCube Collaboration 2022). We plot the IceCube 90% CL upper limit of all flavor neutrinos for index $p = 1.5$ in Figure 2, which shows that our predicted neutrino flux does not violate the IceCube upper limit, assuming the flavor ratio as $1 : 1 : 1$ after oscillation.

The Giant Radio Array for Neutrino Detection (GRAND, Álvarez-Muñiz et al. (2020)) is a scheduled detector for high energy particles with energy larger than 10^{17} eV, including neutrinos, UHECRs, and gamma-rays. The full planned configuration of GRAND will cover an area of 200,000 km². The GRAND sensitivity for transient neutrino flares with zenith angle of 90° are plotted in Figure 2. Before taking account of the synchrotron cooling of pions and muons, the neutrino spectrum peaks around $10^{17} - 10^{18}$ eV, which is just the sensitive band of GRAND. However, by taking account of the synchrotron cooling suppression, the neutrino fluence is suppressed in the sensitive band of GRAND. Hence, if adopting the equilibrium energy of magnetic field $\epsilon_B = 10^{-2}$, neutrinos from GRB 221009A-like event will not be able to be detected by GRAND, as shown in Fig. 2. If a lower equilibrium energy of magnetic field is assumed, for instance, $\epsilon_B = 10^{-4}$, the energy of neutrinos can reach the GRAND's threshold. Therefore, future observations of GRAND on neutrinos from other GRBs similar to GRB 221009A would constrain the magnetic field in the burst, and further constrain the acceleration mechanism of cosmic rays and the GRB central engine model.

5. PROPAGATION IN THE INTER-GALACTIC SPACE AND IN THE MILKY WAY

Protons injected into the inter-galactic space are contributed by two components, as mentioned above, one component is protons directly escaping from the burst, with energy above 300 EeV, and the other is the neutron-decay-induced protons, with energy above 10 EeV. Assuming that protons accelerated in the burst follows Eq. (11) with $p = 2$,

as shown by the dashed-dotted line in Figure 3, the spectra of the directly escaping protons and the neutron-decay-induced protons injected into the inter-galactic space would follow the dark orange dotted line and the purple dotted line in Figure 3, respectively.

In the inter-galactic space, protons are deflected by the intergalactic magnetic field (IGMF) randomly. The corresponding deflection and time delay of protons depends on the strength of the IGMF. The rms of the deflection angle is estimated as (Finley 2006)

$$\theta_{\text{rms,IG}} = 2.9 \times 10^{-6\circ} \varepsilon_{p,19.5}^{-1} B_{\text{IG},-16} \left(\frac{\lambda_{\text{IG}}}{1 \text{ Mpc}} \right)^{1/2} \left(\frac{D}{745 \text{ Mpc}} \right)^{1/2}, \quad (17)$$

where B_{IG} and λ_{IG} are the rms strength and the coherence length of the IGMF, and D is the distance between the source and the MW. The time delay due to the IGMF is about (Alcock & Hatchett 1978; Alves Batista 2022)

$$\Delta t_{\text{IG}} \simeq 16 \text{ s } \varepsilon_{p,19.5}^{-2} B_{\text{IG},-16}^2 \frac{\lambda_{\text{IG}}}{1 \text{ Mpc}} \left(\frac{D}{745 \text{ Mpc}} \right)^2. \quad (18)$$

If $B_{\text{IG}} \lesssim 10^{-13} \text{ G}$ and $\lambda_{\text{IG}} \lesssim 1 \text{ Mpc}$, there are $\theta_{\text{rms,IG}} \ll \theta_j$ and $\Delta t_{\text{IG}} < 5 \text{ yr}$ for protons with energy larger than 10 EeV, therefore, the fluence of protons arriving at the MW within 5 years would not be suppressed by the deflection of the IGMF significantly. A $\sim 400 \text{ GeV}$ photon to the direction of GRB 221009A was detected by *Fermi*-LAT with a time delay of 0.4 days, suggesting an IGMF strength $B_{\text{IG}} \sim 4 \times 10^{-17} \text{ G}$ (Xia et al. 2022), which is consistent with constraints made from TeV blazars (Dermer et al. 2011; Podlesnyi et al. 2022). Adopting $B_{\text{IG}} \sim 4 \times 10^{-17} \text{ G}$, in the inter-galactic space, protons with energy larger than 10 EeV are deflected by extremely small angles and short time delays, which can be ignored for the detection of UHECRs on Earth.

A 3D simulation on protons propagating in the inter-galactic space is operated via the software CRPROPA 3.2 (Alves Batista et al. 2016, 2022), taking account of interactions with the EBL (Gilmore et al. 2012) and CMB photons, including photo-pion productions, photo-disintegration, and electron-pair productions. The direct escape protons and neutron-induced protons are injected from a source at a comoving distance 647 Mpc to a spherical observer with a radius of $R_{\text{obs}} = 100 \text{ kpc}$ ². In the 3D simulation, we assume a Kolmogorov-type turbulent magnetic field with the rms strength of $B_{\text{rms}} = 4 \times 10^{-17} \text{ G}$ and the coherence length of $l_c = 192 \text{ kpc}$. We consider a grid of 256^3 cells covering a total volume of $\sim (7.7 \text{ Mpc})^3$. The grid is assumed to be periodically repeated to cover the whole simulation region. The Cash-Karp method (Cash & Karp 1990) is adopted for simulating charged particle propagation in a magnetic field. The simulation shows that protons with energy larger than 30 EeV lose more than 50% energy after propagating a comoving distance of 624.7 Mpc. Therefore, the fluence of ultra-high-energy protons arriving at the edge of the MW is significantly suppressed. Most of the UHECRs from GRB 221009A lose their energy to $\lesssim 60 \text{ EeV}$ after propagating in the inter-galactic space. The protons arriving at the edge of the MW peak around the energy of 30 – 40 EeV with the spectra shown by solid lines in Figure 3. From Figure 3, one can tell that, the contribution from neutron-decay-induced protons (the purple solid line) is dominated over the contribution from the direct escape protons (the dark orange solid line).

For the propagation of UHECRs in the MW, the energy loss is negligible, and the GMF model we adopt follows Jansson & Farrar (2012a,b)’s model, including the random large-scale and turbulent small-scale components. We derive a map of protons arriving at Earth following the probability distribution of UHECRs after propagating in the Galactic magnetic field (GMF), via applying Galactic lenses in CRPROPA 3.2 (Alves Batista et al. 2022) on protons that arrive at the edge of the MW. In Figure 4, we plot the map of 1000 UHECRs observed on Earth, with the energy spectral shape of UHECRs at the edge of the MW following the summed spectrum of the two solid lines shown in Figure 3. We backtrack anti-protons from Earth to the edge of the MW at 20 kpc adopting the Cash-Karp propagation method (Cash & Karp 1990) via CRPROPA 3.2, to measure the time delay Δt caused by the Jansson & Farrar (2012a,b) GMF model and the fraction of protons that arriving at Earth within a time delay $f(\Delta t)$. The time delay Δt and deflection angles θ of those protons are plotted in Figure 5, which indicates that, as time increases, protons arriving at Earth have a tendency to distribute around the direction of the GRB within a larger deflection angle. The solid angle $\Omega_{\text{max}}(\Delta t)$ is calculated corresponding to the circle region around the GRB with a radius of the maximum deflection angle $\theta_{\text{max}}(\Delta t)$. Values of $f(\Delta t)$ and the expected solid angle $\Omega_{\text{max}}(\Delta t)$ for the time delay Δt

² The input comoving distance of GRB 221009A is calculated via taking a flat Λ CDM cosmology with $H_0 = 67.4 \text{ kms}^{-1} \text{ Mpc}^{-1}$ and $\Omega_M = 0.315$ (Planck Collaboration et al. 2020).

derived via our simulations on backtracking 2×10^6 anti-protons in the GMF, are listed in Table 2. In reality, the solid angle could be measured from the detected excess of UHECRs around the direction of the GRB.

6. RESULTS AND PROSPECTS

The expected counts of protons with the energy of > 10 EeV from the GRB detected by October of the year $2022 + \Delta t$ can be calculated as

$$N_s(\Delta t) = 163 f(\Delta t) \xi_{p,0} \frac{A_{\text{eff}}}{310 \text{ km}^2}. \quad (19)$$

where A_{eff} is the annual exposure of the detector.

We assume the background spectrum is the same as the spectrum of the isotropic UHECRs detected by the PAO. The expected UHECR background counts within a solid angle $\Omega_{\text{max}}(\Delta t)$ around the GRB integrated over time by October of the year $2022 + \Delta t$ can be estimated via ³

$$N_b(\Delta t) = A_{\text{eff}} \int_0^{\Delta t} \int_{10 \text{ EeV}}^{\infty} J_{\text{CR}}(\varepsilon_{\text{CR}}) \Omega_{\text{max}}(dt) d\varepsilon_{\text{CR}} dt, \quad (20)$$

where $J_{\text{CR}}(\varepsilon_{\text{CR}})$ follows the spectrum of isotropic UHECRs detected by the PAO, as described by Eq. (8) in Aab et al. (2020), in units of $\text{km}^{-2} \text{sr}^{-1} \text{yr}^{-1} \text{EeV}^{-1}$.

The statistical significance of the UHECR excess can be calculated via the Li & Ma method (Li & Ma 1983; Abbasi et al. 2014)

$$S_{\text{LM}} = \sqrt{2} \left[N_{\text{on}} \ln \left(\frac{2N_{\text{on}}}{N_{\text{on}} + N_{\text{off}}} \right) + N_{\text{off}} \ln \left(\frac{2N_{\text{off}}}{N_{\text{on}} + N_{\text{off}}} \right) \right]^{1/2} \quad (21)$$

where $N_{\text{on}} = N_s + N_b$ and $N_{\text{off}} = N_b$.

The Pierre Auger Observatory (PAO), Telescope Array (TA), and TA $\times 4$ are the largest UHECR detectors in the world. The exposure of the cosmic ray detector depends on the declination of the arriving UHECRs. According to the directional exposure for surface detectors of the PAO and TA shown in the left panel of Figure 1 in Biteau et al. (2019), the averaged annual exposure of the PAO and TA for the GRB's declination 19.7° is adopted as $\sim 310 \text{ km}^2$ and $\sim 170 \text{ km}^2$, with compiled dataset of events with energies $E > 8.9$ EeV and $E > 10$ EeV, respectively. The exposure of fully completed TA $\times 4$ is approximately 4 times the TA exposure, while so far about half of the full TA $\times 4$ is completed (Kido 2023). Counts of GRB UHECRs that will be detected by the PAO and the full TA $\times 4$, for the baryon loading factor $\xi_p = 1$, are plotted in Figure 6. The significance of the PAO and TA $\times 4$ detection peaks around 2030-2035, reaches 4.3σ and 6.4σ , respectively, and then decreases since the solid angle of the arriving UHECRs increases, more background is included, as the time increases. By October 2027, after 5-year observations, the PAO and the full TA $\times 4$ can detect ~ 17 and ~ 36 GRB UHECRs (plus ~ 5 and ~ 11 background UHECRs) with energy larger than 10 EeV and the maximum deflection angle θ_{max} of $\sim 5^\circ$ around the direction of the GRB. The corresponding significance of the excess is estimated to be $\sim 3.4 \sigma$ and 5.0σ , respectively. If combining the PAO and the fully completed TA $\times 4$ data, the combined significance would become higher, which would exceed 5σ by 2027.

The annual exposure of GRAND for UHECRs from GRB 221009A is about 10 times the PAO according to Figure 10 in the GRAND white paper (Álvarez-Muñiz et al. 2020). If the construction of GRAND can be completed before 2035, GRAND can detect ~ 148 GRB UHECRs plus ~ 347 background UHECRs with the energy of > 10 EeV around the GRB, with 8-year operation from the beginning of 2035 to the end of 2042, for $\xi_p = 1$, with a significance of the excess as $\sim 5.1 \sigma$. The projected significance of the UHECR excess measurable for these three detectors is shown in Figure 6, and the prospects are indeed promising.

In He et al. (2016), a Monte Carlo Bayesian method is proposed to study the correlation between UHECRs and source candidates, via studying the spatial distribution of UHECRs with different energies. In the future, we can take into account not only the spatial distribution of UHECRs depending on the energy but also the temporal information of the arriving UHECRs, to further check the correlation between the detected UHECRs and the GRB at high statistics.

In this work, we adopt a high bulk Lorentz factor ~ 500 , as suggested by LHAASO observations on the afterglow. With a typical variability timescale of ~ 0.082 s, as observed by *Fermi*-GBM, we then take an energy dissipation radius $R \sim 10^{15} \text{ cm}$, where protons are accelerated. A large energy dissipation radius and a high bulk Lorentz factor of the

³ Here we calculate the integration adopting half-a-year bins.

ejecta are helpful in enhancing the maximum energy of the accelerated protons, as indicated by Eq. (2), and further leads to a high flux of observed UHECRs. Interestingly, a large energy dissipation radius of $\sim 10^{15}$ cm may challenge the standard fireball internal shock model unless just a small fraction of electrons have been accelerated otherwise the synchrotron radiation of the shocked electrons will not be able to peak at MeV energies. Instead, a large energy dissipation radius of $10^{15} - 10^{16}$ cm is natural for a Poynting-flux-dominated GRB outflow (e.g., Fan et al. 2005; Zhang & Yan 2011; Kumar & Zhang 2015). Indeed, recently, Zhang et al. (2023) suggested that the ejecta of GRB 221009A was composed of a narrow ($\sim 0.6^\circ$ half opening angle) Poynting-flux-dominated outflow composition and a broader matter-dominated jet wing. In the future, a successful detection of the UHECR outburst from GRB 221009A will not only directly establish the GRB-UHECR connection, but also provide us a valuable chance to measure or stringently constrain the IGMF and the GMF, and key parameters of the GRB physics, such as the energy dissipation radius, the bulk Lorentz factor and the baryon loading factor of the jet, and further reveal the radiation mechanism and the central engine of the GRB.

Table 1. Adopted Parameters of GRB 221009A.

Descriptions	Symbols	Values
Redshift	z	0.151
Dissipation radius	R	10^{15} cm
Low energy photon index ^a	α	0.76
High-energy photon index ^a	β	2.13
Minimum energy of photon spectrum ^a	$\varepsilon_{\gamma,\min}$	20 keV
Maximum energy of photon spectrum ^a	$\varepsilon_{\gamma,\max}$	10 MeV
Peak energy of photon spectrum ^a	$\varepsilon_{\gamma,b}$	3 MeV
Calibration luminosity ^b	L_γ	1×10^{54} erg s ⁻¹
Bulk Lorentz factor	Γ	500
Baryon loading factor	ξ_p	1
Proton index	p	2
Minimum energy of proton spectrum	$\varepsilon_{p,\min}$	9.8×10^{10} eV
Maximum energy of proton spectrum	$\varepsilon_{p,\max}$	1.2×10^{21} eV
Fraction of magnetic field energy	ϵ_B	0.01
Fraction of electron energy	ϵ_e	0.1
Total radiation energy	$E_{\gamma,\text{iso}}$	10^{55} erg

^a Parameters for the brightest emission from $T_0 + 225.024$ s to $T_0 + 233.216$ s in the second pulse are listed (Frederiks et al. 2023), with $T_0 = 47821.648$ s UT (13:17:01.648) on 2022 October 9 as the Konus-WIND trigger time.

^b The luminosity at 20 keV–10 MeV.

Table 2. The time delay Δt , the fraction of arriving UHECRs $f(\Delta t)$, the solid angle $\Omega_{\max}(\Delta t)$, and the significance detected by the PAO and TA \times 4 by the October of certain years, assuming the baryon loading factor $\xi_p = 1$.

Time	$\Delta t[\text{yr}]$	$f(\Delta t)$	$\Omega_{\max}(\Delta t)[\text{sr}]$	PAO Significance $[\sigma]$	TA \times 4 Significance $[\sigma]$
2025.10	3	3.5%	0.013	1.9	2.8
2027.10	5	10.2%	0.020	3.4	5.0
2029.10	7	15.5%	0.027	4.0	5.8
2031.10	9	19.4%	0.034	4.2	6.2
2033.10	11	22.7%	0.040	4.3	6.3
2035.10	13	25.7%	0.046	4.3	6.4
2037.10	15	29.8%	0.059	4.1	6.1

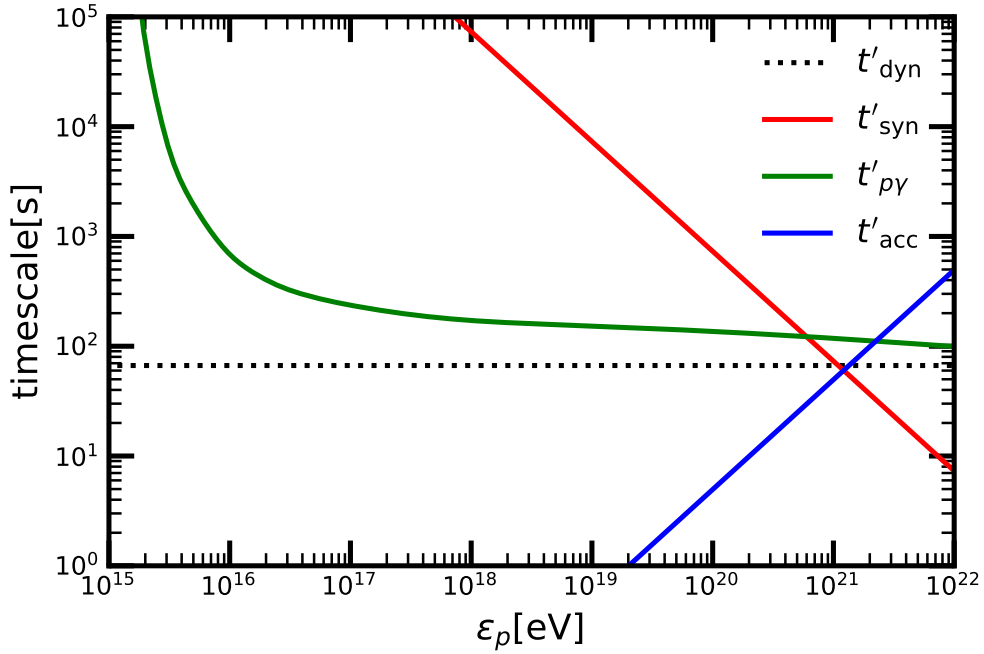


Figure 1. Various timescales as functions of the proton energy. All the timescales are measured in the comoving frame of the GRB outflow. The adopted parameters are listed in the Table 1.

This work is supported by Project for Young Scientists in Basic Research of Chinese Academy of Sciences (No. YSBR-061), and by NSFC under the grants of No. 12173091, No. 11921003, No.12321003 and No. 12333006.

Software: ASTROPY (ASTROPY COLLABORATION ET AL. 2013, 2018), CRPROPA 3.2 (ALVES BATISTA ET AL. 2016), SOPHIA (MÜCKE ET AL. 2000A)

REFERENCES

- Aab, A., Abreu, P., Aglietta, M., et al. 2020, PhRvD, 102, 062005, doi: [10.1103/PhysRevD.102.062005](https://doi.org/10.1103/PhysRevD.102.062005)
- Abbasi, R., Ackermann, M., Adams, J., et al. 2022, ApJ, 939, 116, doi: [10.3847/1538-4357/ac9785](https://doi.org/10.3847/1538-4357/ac9785)
- . 2023, ApJL, 946, L26, doi: [10.3847/2041-8213/acc077](https://doi.org/10.3847/2041-8213/acc077)
- Abbasi, R. U., Abe, M., Abu-Zayyad, T., et al. 2014, ApJL, 790, L21, doi: [10.1088/2041-8205/790/2/L21](https://doi.org/10.1088/2041-8205/790/2/L21)
- Ai, S., & Gao, H. 2023, ApJ, 944, 115, doi: [10.3847/1538-4357/acb3bf](https://doi.org/10.3847/1538-4357/acb3bf)
- Alcock, C., & Hatchett, S. 1978, ApJ, 222, 456, doi: [10.1086/156159](https://doi.org/10.1086/156159)
- Álvarez-Muñiz, J., Alves Batista, R., Balagopal V., A., et al. 2020, Science China Physics, Mechanics, and Astronomy, 63, 219501, doi: [10.1007/s11433-018-9385-7](https://doi.org/10.1007/s11433-018-9385-7)
- Alves Batista, R. 2022, arXiv e-prints, arXiv:2210.12855, doi: [10.48550/arXiv.2210.12855](https://doi.org/10.48550/arXiv.2210.12855)
- Alves Batista, R., Dundovic, A., Erdmann, M., et al. 2016, JCAP, 2016, 038, doi: [10.1088/1475-7516/2016/05/038](https://doi.org/10.1088/1475-7516/2016/05/038)
- Alves Batista, R., Becker Tjus, J., Dörner, J., et al. 2022, JCAP, 2022, 035, doi: [10.1088/1475-7516/2022/09/035](https://doi.org/10.1088/1475-7516/2022/09/035)
- An, Z.-H., Antier, S., Bi, X.-Z., et al. 2023, arXiv e-prints, arXiv:2303.01203, doi: [10.48550/arXiv.2303.01203](https://doi.org/10.48550/arXiv.2303.01203)
- Astropy Collaboration, Robitaille, T. P., Tollerud, E. J., et al. 2013, A&A, 558, A33, doi: [10.1051/0004-6361/201322068](https://doi.org/10.1051/0004-6361/201322068)
- Astropy Collaboration, Price-Whelan, A. M., Sipőcz, B. M., et al. 2018, AJ, 156, 123, doi: [10.3847/1538-3881/aabc4f](https://doi.org/10.3847/1538-3881/aabc4f)
- Baerwald, P., Bustamante, M., & Winter, W. 2013, ApJ, 768, 186, doi: [10.1088/0004-637X/768/2/186](https://doi.org/10.1088/0004-637X/768/2/186)
- Bissaldi, E., Omodei, N., Kerr, M., & Fermi-LAT Team. 2022, GRB Coordinates Network, 32637, 1

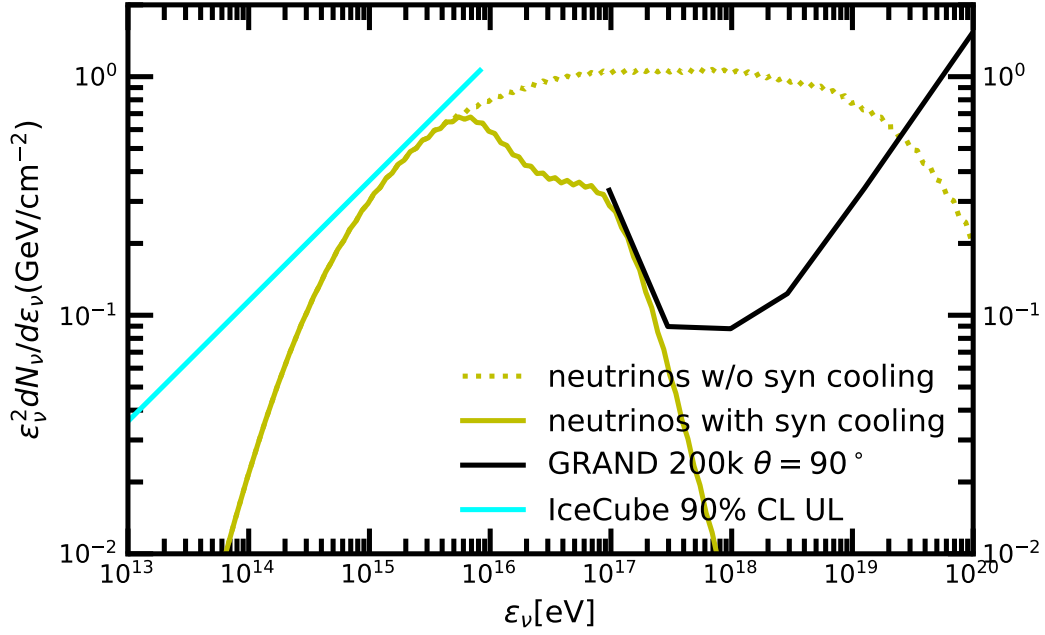


Figure 2. The fluence of all flavor neutrinos from the source, adopting parameters as in Table 1. The dark green dotted line is the neutrino spectrum without considering the synchrotron cooling of pions and muons, and the dark green solid line is the one considering the synchrotron cooling effect. The black solid line is the sensitivity of GRAND detecting neutrinos with a zenith angle of $\theta = 90^\circ$ assuming null background. The cyan solid line is the upper limit flux of all-flavor neutrinos in the IceCube’s 3 hours FRA by assuming the spectral index as $p = 1.5$.

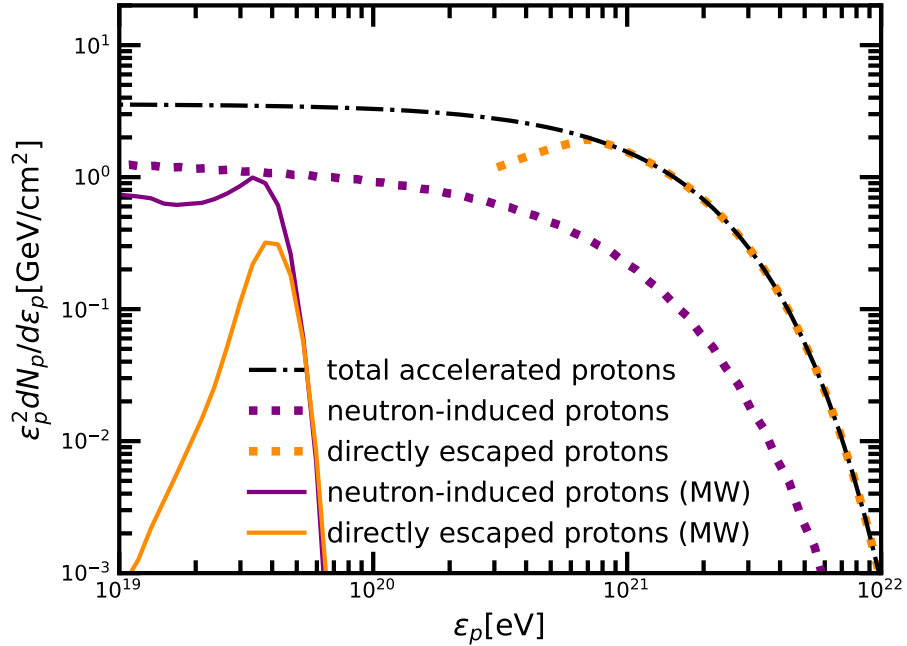


Figure 3. The spectra of protons involved in this work. The dash-dotted line, dotted lines, and solid lines represent protons accelerated in the burst, injected to the inter-galactic space, and arriving at the edge of the MW, respectively.

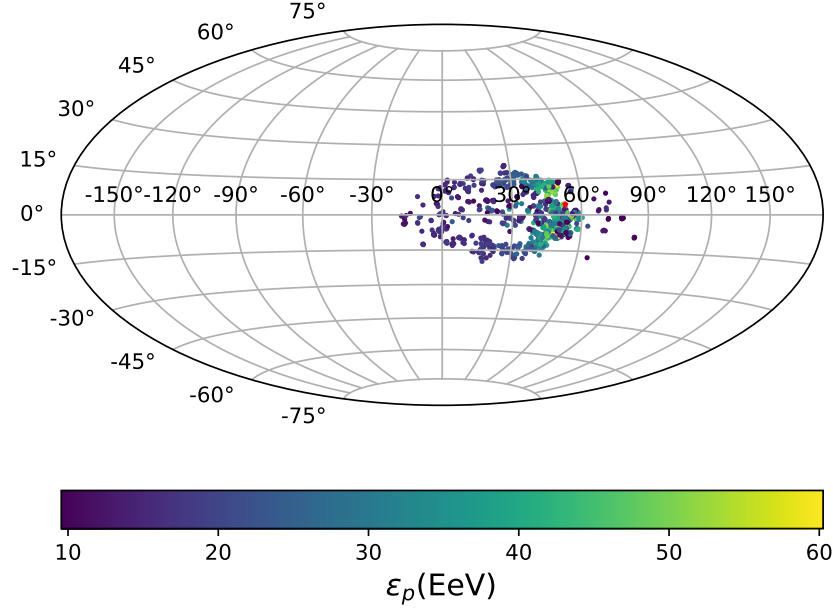


Figure 4. The expected arrival distribution of 1000 UHECRs from GRB 221009A in the Galactic coordination, in the Hammer projection. Colors represent energies of arriving UHECRs. The red star denotes the coordinate of GRB 221009A.

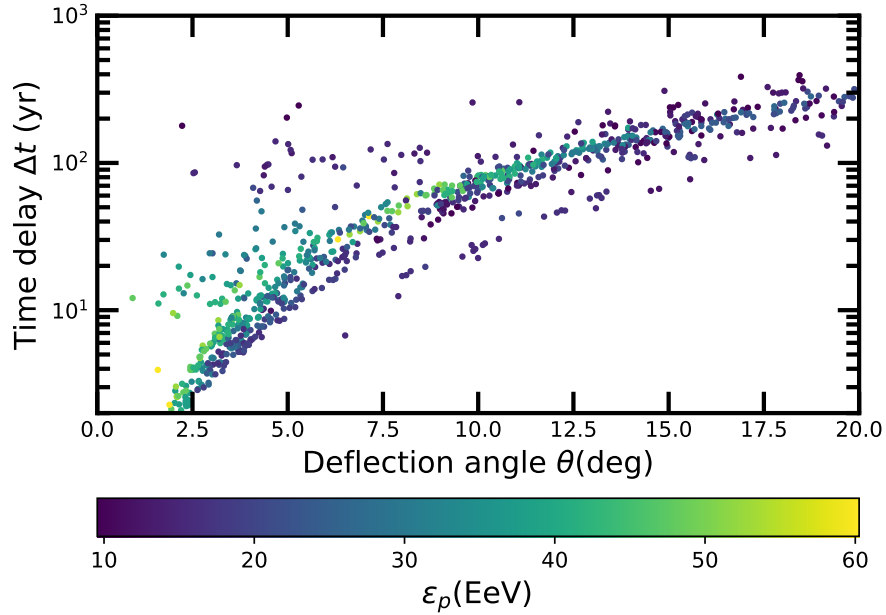


Figure 5. The expected time delay and deflection angles of the arriving UHECRs from GRB 221009A. The deflection and the time delay are mainly contributed by the Galactic magnetic fields. Colors represent energies of arriving UHECRs.

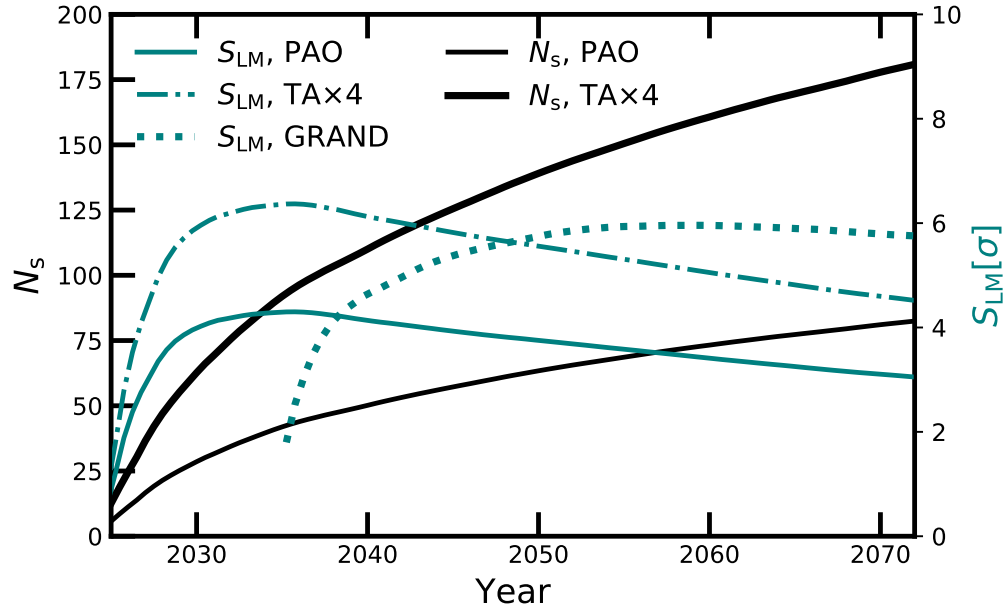


Figure 6. The prospect of detecting the UHECR outburst from GRB 221009A. The expected integral counts detected by the PAO and the full TA×4, as a function of the time since the trigger time of GRB 221009A, are shown in solid lines. The teal lines denote the significance of the UHECR excess, detected by the PAO, the full TA×4 and GRAND, respectively. The X-axis starts from the year of 2025.

- Burns, E., Svinkin, D., Fenimore, E., et al. 2023, *ApJL*, 946, L31, doi: [10.3847/2041-8213/acc39c](https://doi.org/10.3847/2041-8213/acc39c)
- Cao, Z., et al. 2023a, *Science*, 380, adg9328, doi: [10.1126/science.adg9328](https://doi.org/10.1126/science.adg9328)
- . 2023b. <https://arxiv.org/abs/2310.08845>
- Cash, J. R., & Karp, A. H. 1990, *ACM Transactions on Mathematical Software*, 16, 201–222, doi: [10.1145/79505.79507](https://doi.org/10.1145/79505.79507)
- Castro-Tirado, A. J., Sanchez-Ramirez, R., Hu, Y. D., et al. 2022, *GRB Coordinates Network*, 32686, 1
- Das, S., & Razzaque, S. 2023, *A&A*, 670, L12, doi: [10.1051/0004-6361/202245377](https://doi.org/10.1051/0004-6361/202245377)
- de Ugarte Postigo, A., Izzo, L., Pugliese, G., et al. 2022, *GRB Coordinates Network*, 32648, 1
- Dermer, C. D., & Atoyan, A. 2006, *New Journal of Physics*, 8, 122, doi: [10.1088/1367-2630/8/7/122](https://doi.org/10.1088/1367-2630/8/7/122)
- Dermer, C. D., Cavadini, M., Razzaque, S., et al. 2011, *ApJL*, 733, L21, doi: [10.1088/2041-8205/733/2/L21](https://doi.org/10.1088/2041-8205/733/2/L21)
- Dermer, C. D., Murase, K., & Takami, H. 2012, *ApJ*, 755, 147, doi: [10.1088/0004-637X/755/2/147](https://doi.org/10.1088/0004-637X/755/2/147)
- Fan, Y. Z., Zhang, B., & Proga, D. 2005, *ApJL*, 635, L129, doi: [10.1086/499489](https://doi.org/10.1086/499489)
- Finley, C. B. 2006, PhD thesis, Columbia University, New York
- Frederiks, D., Svinkin, D., Lysenko, A. L., et al. 2023, *ApJL*, 949, L7, doi: [10.3847/2041-8213/acd1eb](https://doi.org/10.3847/2041-8213/acd1eb)
- Gilmore, R. C., Somerville, R. S., Primack, J. R., & Domínguez, A. 2012, *MNRAS*, 422, 3189, doi: [10.1111/j.1365-2966.2012.20841.x](https://doi.org/10.1111/j.1365-2966.2012.20841.x)
- Harari, D., Mollerach, S., Roulet, E., & Sánchez, F. 2002, *Journal of High Energy Physics*, 2002, 045, doi: [10.1088/1126-6708/2002/03/045](https://doi.org/10.1088/1126-6708/2002/03/045)
- He, H.-N., Kusenko, A., Nagataki, S., et al. 2016, *PhRvD*, 93, 043011, doi: [10.1103/PhysRevD.93.043011](https://doi.org/10.1103/PhysRevD.93.043011)
- He, H.-N., Liu, R.-Y., Wang, X.-Y., et al. 2012, *ApJ*, 752, 29, doi: [10.1088/0004-637X/752/1/29](https://doi.org/10.1088/0004-637X/752/1/29)
- IceCube Collaboration. 2022, *GRB Coordinates Network*, 32665, 1
- Icecube Collaboration, Abbasi, R., Abdou, Y., et al. 2012, *Nature*, 484, 351, doi: [10.1038/nature11068](https://doi.org/10.1038/nature11068)
- Isravel, H., Begue, D., & Pe’er, A. 2023, *Astrophys. J.*, 956, 12, doi: [10.3847/1538-4357/acefcd](https://doi.org/10.3847/1538-4357/acefcd)
- Jansson, R., & Farrar, G. R. 2012a, *ApJ*, 757, 14, doi: [10.1088/0004-637X/757/1/14](https://doi.org/10.1088/0004-637X/757/1/14)
- . 2012b, *ApJL*, 761, L11, doi: [10.1088/2041-8205/761/1/L11](https://doi.org/10.1088/2041-8205/761/1/L11)
- Kido, E. 2023, in *European Physical Journal Web of Conferences*, Vol. 283, *European Physical Journal Web of Conferences*, 06003, doi: [10.1051/epjconf/202328306003](https://doi.org/10.1051/epjconf/202328306003)
- Kumar, P., & Zhang, B. 2015, *PhR*, 561, 1, doi: [10.1016/j.physrep.2014.09.008](https://doi.org/10.1016/j.physrep.2014.09.008)
- Lee, S., Olinto, A. V., & Sigl, G. 1995, *ApJL*, 455, L21, doi: [10.1086/309812](https://doi.org/10.1086/309812)
- Levan, A. J., Lamb, G. P., Schneider, B., et al. 2023, *ApJL*, 946, L28, doi: [10.3847/2041-8213/acc2c1](https://doi.org/10.3847/2041-8213/acc2c1)
- Li, T. P., & Ma, Y. Q. 1983, *ApJ*, 272, 317, doi: [10.1086/161295](https://doi.org/10.1086/161295)
- Liu, R.-Y., Zhang, H.-M., & Wang, X.-Y. 2023, *ApJL*, 943, L2, doi: [10.3847/2041-8213/acaf5e](https://doi.org/10.3847/2041-8213/acaf5e)
- Malesani, D. B., Levan, A. J., Izzo, L., et al. 2023, *arXiv e-prints*, arXiv:2302.07891, doi: [10.48550/arXiv.2302.07891](https://doi.org/10.48550/arXiv.2302.07891)
- Mannheim, K., Protheroe, R. J., & Rachen, J. P. 2000, *PhRvD*, 63, 023003, doi: [10.1103/PhysRevD.63.023003](https://doi.org/10.1103/PhysRevD.63.023003)
- Mészáros, P. 2002, *ARA&A*, 40, 137, doi: [10.1146/annurev.astro.40.060401.093821](https://doi.org/10.1146/annurev.astro.40.060401.093821)
- Mirabal, N. 2023, *MNRAS*, 519, L85, doi: [10.1093/mnras/slac157](https://doi.org/10.1093/mnras/slac157)
- Mücke, A., Engel, R., Rachen, J. P., Protheroe, R. J., & Stanev, T. 2000a, *Computer Physics Communications*, 124, 290, doi: [10.1016/S0010-4655\(99\)00446-4](https://doi.org/10.1016/S0010-4655(99)00446-4)
- Mücke, A., Rachen, J. P., Engel, R., Protheroe, R. J., & Stanev, T. 2000b, *Nuclear Physics B Proceedings Supplements*, 80, 08/10, doi: [10.48550/arXiv.astro-ph/9905153](https://doi.org/10.48550/arXiv.astro-ph/9905153)
- Murase, K., Mukhopadhyay, M., Kheirandish, A., Kimura, S. S., & Fang, K. 2022, *ApJL*, 941, L10, doi: [10.3847/2041-8213/aca3ae](https://doi.org/10.3847/2041-8213/aca3ae)
- Pillera, R., Bissaldi, E., Omodei, N., La Mura, G., & Longo, F. 2022, *The Astronomer’s Telegram*, 15656, 1
- Planck Collaboration, Aghanim, N., Akrami, Y., et al. 2020, *A&A*, 641, A6, doi: [10.1051/0004-6361/201833910](https://doi.org/10.1051/0004-6361/201833910)
- Podlesnyi, E. I., Dzhatdov, T. A., & Galkin, V. I. 2022, *MNRAS*, 516, 5379, doi: [10.1093/mnras/stac2509](https://doi.org/10.1093/mnras/stac2509)
- Rudolph, A., Petropoulou, M., Winter, W., & Bošnjak, Ž. 2023, *ApJL*, 944, L34, doi: [10.3847/2041-8213/acb6d7](https://doi.org/10.3847/2041-8213/acb6d7)
- Veres, P., Meegan, C., & Fermi GBM Team. 2022, *GRB Coordinates Network*, 33125, 1
- Vietri, M. 1995, *ApJ*, 453, 883, doi: [10.1086/176448](https://doi.org/10.1086/176448)
- Wang, K., Liu, R.-Y., Dai, Z.-G., & Asano, K. 2018, *ApJ*, 857, 24, doi: [10.3847/1538-4357/aab667](https://doi.org/10.3847/1538-4357/aab667)
- Wang, K., Ma, Z.-P., Liu, R.-Y., et al. 2023, *arXiv e-prints*, arXiv:2302.11111, doi: [10.48550/arXiv.2302.11111](https://doi.org/10.48550/arXiv.2302.11111)
- Waxman, E. 1995, *PhRvL*, 75, 386, doi: [10.1103/PhysRevLett.75.386](https://doi.org/10.1103/PhysRevLett.75.386)
- Waxman, E., & Bahcall, J. 1997, *PhRvL*, 78, 2292, doi: [10.1103/PhysRevLett.78.2292](https://doi.org/10.1103/PhysRevLett.78.2292)
- Williams, M. A., Kennea, J. A., Dichiaro, S., et al. 2023, *ApJL*, 946, L24, doi: [10.3847/2041-8213/acbcd1](https://doi.org/10.3847/2041-8213/acbcd1)

- Workman, R. L., Burkert, V. D., Crede, V., et al. 2022, Progress of Theoretical and Experimental Physics, 2022, 083C01, doi: [10.1093/ptep/ptac097](https://doi.org/10.1093/ptep/ptac097)
- Xia, Z.-Q., Wang, Y., Yuan, Q., & Fan, Y.-Z. 2022, arXiv e-prints, arXiv:2210.13052, doi: [10.48550/arXiv.2210.13052](https://doi.org/10.48550/arXiv.2210.13052)
- Zhang, B., Wang, X.-Y., & Zheng, J.-H. 2023, arXiv e-prints, arXiv:2311.14180, doi: [10.48550/arXiv.2311.14180](https://doi.org/10.48550/arXiv.2311.14180)
- Zhang, B., & Yan, H. 2011, ApJ, 726, 90, doi: [10.1088/0004-637X/726/2/90](https://doi.org/10.1088/0004-637X/726/2/90)
- Zhang, B. T., Murase, K., Ioka, K., et al. 2023a, Astrophys. J. Lett., 947, L14, doi: [10.3847/2041-8213/acc79f](https://doi.org/10.3847/2041-8213/acc79f)
- Zhang, B. T., Murase, K., Ioka, K., & Zhang, B. 2023b, <https://arxiv.org/abs/2311.13671>
- Zhang, B. T., Murase, K., Kimura, S. S., Horiuchi, S., & Mészáros, P. 2018, PhRvD, 97, 083010, doi: [10.1103/PhysRevD.97.083010](https://doi.org/10.1103/PhysRevD.97.083010)